PERGAMON

International Journal of Rock Mechanics & Mining Sciences 38 (2001) 379–397

International Journal of
Rock Mechanics
and Mining Sciences

www.elsevier.com/locate/ijrmms

A three-dimensional slope stability analysis method using the upper bound theorem
Part II: numerical approaches, applications and extensions

Zuyu Chen[a,b,*], Jian Wang[a], Yujie Wang[c], Jian-Hua Yin[c], Chris Haberfield[d]

[a] *Department of Hydraulic Engineering, Tsinghua University, People's Republic of China*
[b] *China Institute of Water Resources and Hydropower Research, 20, West Chegongzhuang Road, P.O. Box 366, Beijing 100044, People's Republic of China*
[c] *Department of Civil and Structural Engineering, The Hong Kong Polytechnic University, Hong Kong*
[d] *Department of Civil Engineering, P.O. Box 3800, Australia*

Accepted 8 January 2001

Abstract

The second part of this paper provides the numerical procedures that implement the three-dimensional upper-bound slope stability analysis method described in Part I. A three-dimensional failure surface is generated by elliptical lines based on the slip surface in the neutral plane and extended in the z direction. This failure surface is mathematically represented by a series of variables including the co-ordinates of the nodal points that define the slip surface at the neutral plane, the inclinations of the row-to-row interfaces and the coefficients that define the ratio of the long axis over the low one of the elliptic. A method of optimisation is followed in order to find a set of these variables that offers the minimum factor of safety. A computer program EMU-3D is coded to perform the calculation for practical problems. Applications and extensions of the method presented in this paper include a case study of the Tianshenqiao Landslide, the stability analysis of the right abutment of the Xiaowan arch dam, and the portal of the Hongjiadu hydropower project.

Keywords: Slope stability analysis; Three-dimensional analysis; Upper bound theorem; The method of optimisation; Arch dam abutment; Tunnel portals

1. Introduction

The three-dimensional (3D) slope stability analysis method proposed in Part I of this paper allows a quick and simple method of determining the factor of safety for a specified slip surface and interface inclinations. However, a practicable and useful 3D method employing this theory requires solutions to the following related numerical problems:

- *Mathematical modelling of failure surfaces and interfaces in three dimensions*. The failure surface of a natural landslide usually exhibits a complex shape, often controlled by geological features. Failure surfaces are not necessarily spherical or log-spiral, as has been employed by some researchers [1,2] but may involve several planar geological structures as part of the slip surface or interfaces. Their mathematical description must offer great flexibility for simulating a generalised failure mode but must involve as few controlling parameters as possible so as to reduce the computational effort when searching for the critical surface and minimum factor of safety. Dividing a failure mass into a series of prisms with inclined interfaces and adopting an appropriate numbering system to identify each part of the slip surface and interfaces will complicate the process even further. In a typical application, the discretisation of three-dimensional topography and geometry may need to be carried out several thousand times during the optimisation process and therefore any

*Corresponding author. China Institute of Water Resources and Hydropower Research, 20, West Chegongzhuang Road, P.O. Box 366, Beijing 100044, People's Republic of China. Tel.: +86-10-685-148-24; fax: +86-10-684-383-17.

E-mail address: chenzy@tsinghua.edu.cn (Z. Chen).

1365-1609/01/$ - see front matter
PII: S1365-1609(01)00013-2

numbering system must be unique and logical so that it can be automatically generated by the computer program.

- *The optimisation methods employed in searching for the critical slip surface*. The upper bound theorem upon which the method is based requires calculation of factors of safety for many possible failure modes until the minimum factor of safety is obtained. Failure to do so will cause an overestimation of the factor of safety. This can be a difficult process even with two-dimensional problems. In three dimensions, the degrees of freedom which need to be optimised increase considerably, thereby significantly increasing the complexity of obtaining the optimum solution. The development and/or application of innovative optimisation methods require special consideration in 3D slope stability analyses.
- *Graphics-based presentation of input and output*. Interpretation and quantification of the topographic and geological information and presentation of the results of the analysis is a vital part of the development of the method. Lam and Fredlund [3] introduced the 'Kriging' technique. The authors' experience has shown that processing the information cross-section by cross-section is a very convenient and reliable way of interpreting the input and output. It allows most of the previous two-dimensional work [4], which has been considerably debugged and updated, to be transferred directly into a 3D program. Treating a 3D profile by a series of cross-sections also enables application of most commercially available 3D graphics programs, such as AUTO CAD, and 3D Studio. The application of these programs considerably reduces the work required to produce meaningful, high quality 3D graphics images.

The authors believe that these problems must be solved through continued application of the method to practical problems. Meanwhile, by applying the method to areas where conventional two-dimensional (2D) methods are inappropriate, the attributes of the 3D method will be illustrated and hence lead to more widespread use. It has been found that rock mechanics and geomechanical engineering offer many potential areas for these extensions. This paper describes the solutions to the numerical problems as well as the applications and extensions of the method to several large-scale hydropower projects that involve possible instability of arch dam abutments and tunnel portals.

2. The generalised three-dimensional slip surface

A 3D slip surface and its related failure mode is developed by the following two types of discretisation:

Type one: The slip surface in each of the cross-sections (i.e. 'z equals constant' section) is specified in a similar manner to that of the 2D approach [4]. A number of nodal points with co-ordinates (x_i, y_i) are connected by either straight lines or smooth curves. The sliding mass at the neutral plane, cross-section 0, is further divided into a series of slices with interfaces inclined at an angle δ_i, (measured from the positive y-axis to the positive x-axis). These are extended in the z direction perpendicular to the $x-y$ plane, cutting the failure mass into prisms. The extended inclined planes are referred to as row-to-row interfaces. The co-ordinate values for top and bottom points of these interfaces are designated $(x^0_{u,}\, y^0_u)$ and $(x^0_{l,}\, y^0_l)$, and are determined by linear interpolation between the co-ordinates of the two adjacent nodal points, x_i and y_i (Fig. 1). The 'z equals constant' cross-sections form column-to-column interfaces. This type of discretisation is suitable for cases where the slip surface is well defined such as in the back analysis of a landslide or in rock slopes in which the structural discontinuities clearly define the failure mode.

Type two: The slip surface is defined by an ellipsoid based on the information of cross-section 0. As with type one, the slip surface on the neutral plane is generated by a series of nodal points with intermediate slices determined by interpolation (Fig. 1(a)). The sliding mass at this section is subdivided by a series of inclined interfaces of length, H. Each interface extends in the z direction to form row-to-row interfaces that are perpendicular to the $x-y$ plane, as shown by cross-section A–A′ in Fig. 1(b). The length of the corresponding interface, h, at the cross-section numbered j, with a

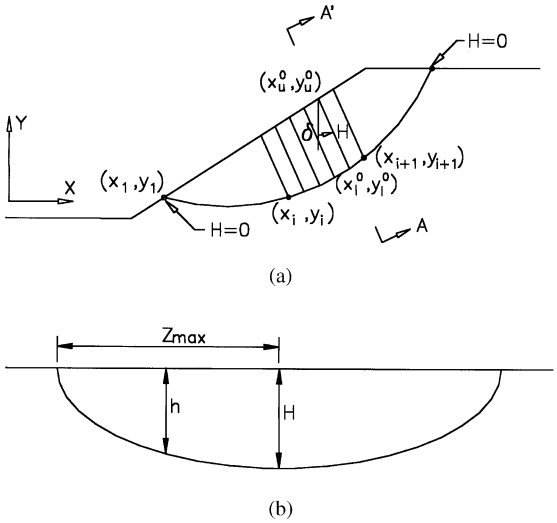

Fig. 1. Developing a generalised three-dimensional slip surface based on the information of the cross-section. (a) The neutral plane; (b) cross-section A–A′, a typical row-to-row interface.

co-ordinate value of z, is given by the following equation:

$$\frac{h^2}{H^2}+\frac{z^2}{[\zeta(H+B)]^2}=1. \tag{1}$$

The two parameters, ζ and B, are included in Eq. (1) to offer a generalised shape of the slip surface and will be explained below. Based on the value of h determined by Eq. (1), the co-ordinates of the points on the slip surface of the cross-section j, represented as $(x_l^j\, y_l^j)$, can be defined as (Fig. 2)

$$\begin{Bmatrix} x_l^j \\ y_l^j \end{Bmatrix} = \begin{Bmatrix} x_u^0 - h\sin\delta_i \\ y_u^0 - h\cos\delta_i \end{Bmatrix}. \tag{2}$$

Note that at both ends of the slip surface on the neutral plane, $H=0$. Therefore, we have $h=0$ at the crown and toe.

In Eq. (1) ζ is a coefficient that defines the ratio of the lengths of the major to minor axis of the ellipsoid on the row-to-row cross-section (Fig. 1(b)). If ζ is unity, the slip surface on this cross-section is circular. For each nodal point that defines the slip surface at cross-section 0, a value of ζ_i is specified. The value of ζ_i for each interface is determined by interpolation, in a similar manner to x_i, y_i and δ_i. The ellipsoid intersects the slope surface at each row-to-row cross-section with a longer axis $z_{\max}$ (Fig. 1(b)) which is determined by the equation

$$z_{\max}=\zeta(H+B). \tag{3}$$

Some slope stability problems require that the slip surface have a specified width at the crown or/and toe. For example, bearing capacity problems require the slip surface to take a specified length at the crown to accommodate the surface load (Fig. 3(a)). The portal of an underground opening always exhibits a cut with a specified width at the toe of the slope (Fig. 3(b)). B is a parameter that allows the slip surface to take a specified length in the z direction at the crown and toe. Since the value of H at the crown or toe is zero, then $z_{\max}=\zeta B$, which is non-zero if both ζ and B are not equal to zero. For instance, to define a slip surface that has a length of $2B_0$ at the crown, values of $\zeta=1$ and $B=B_0$ are used. By specifying $\zeta=0$ for the nodal point at the toe, the slip surface diminishes at the toe. Fig. 3(a) shows a sketch depicting this mode for a bearing capacity problem. On the other hand, taking $\zeta=1$ and $B=B_0$ at the toe will result in a potential failure surface of a tunnel portal as shown in Fig. 3(b).

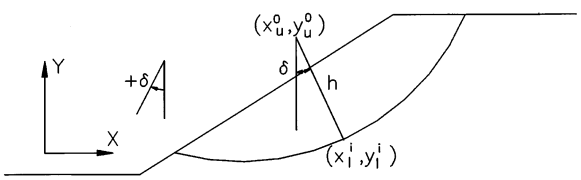

Fig. 2. The slip surface developed by a partly elliptical sphere on a 'z=constant' cross-section.

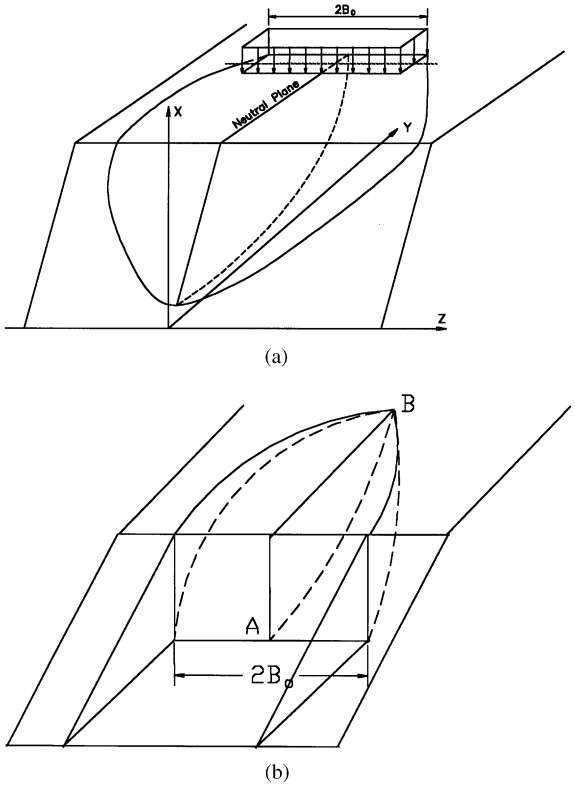

Fig. 3. A sketch of a failure mass created by the discretisation mode type two. (a) The bearing capacity problem; (b) a tunnel portal excavation.

For both types of the discretisation mode, the 'z=constant' cross-sections serve as input for geometry of the slope as well as the column-to-column interfaces. They are parallel to the $x-y$ plane.

3. Search for the critical failure mode

3.1. Variables involved in the optimisation process

The factor of safety for a slip surface defined using Eq. (1) can be expressed as a function of a set of variables related to cross-section 0.

$$F=F(\chi), \tag{4}$$

where

$$\begin{aligned}\chi &= (\chi_1,\ \chi_2,\ \chi_3,\ldots,\chi_n)\\ &= (x_1,\ y_1,\ x_2,\ y_2,\ldots,x_m,\ y_m;\\ &\quad \delta_1,\ \delta_2,\ldots,\delta_m;\ \zeta_1,\ \zeta_2,\ldots,\zeta_m,\ \omega).\end{aligned} \tag{5}$$

The principle of the upper bound method requires the determination of the minimum value of F associated with all possible variables contained on the right-hand side of Eq. (4). At present, the column-to-column interfaces are only allowed to tilt at the same angle ω (defined by Eq. (27) in Part I of this paper) and only

after an initial estimate is made using $\omega = 0$. This means that ω is not involved in the optimisation process.

Some of the variables in Eq. (5) may be fixed due to the particular features of the problem concerned. For example, δ_i will be fixed if the interfaces represent a set of joints of a rock slope. In the back analysis of a slope, since the location of the slip surface is known, x_i and y_i are fixed. Hence, the only variable in Eq. (5) is δ_i.

The discipline of non-linear programming permits a minimum value of F to be obtained for a set of variables that represent a critical failure mode. A number of optimisation methods have been used in 2D slope stability analyses. These can be in general divided into deterministic and probabilistic approaches as will be discussed in the subsequent sections. Both methods have been used in the examples presented in this paper.

3.2. The deterministic optimisation methods

The deterministic methods are traditional approaches in the area of non-linear programming. They can be in turn divided into two categories:

(1) The pattern search method, which approaches the minimum factor of safety by a well designed pattern that compares the objective functions of different variable combinations and determines the best directions to approach a smaller objective function in the next step of iteration. Methods of this kind include the Simplex Method [5], Pattern Search Method [6] and Powell's Method [7] amongst others.

(2) The Newton methods, which theoretically obtain the minimum by finding a set of variables that make all the derivatives of the objective function zero. One example of a method that falls into this category is the Davidon–Fletcher–Powell method [8,9].

The applications of these search techniques to 2D slope stability analyses are discussed extensively in the technical literature [10–14]. In the authors' experience, although the Newton methods have a sound analytical basis, they do not necessarily offer a more efficient way to approach the solution. In many cases different methods give essentially the same solutions and suffer the same problems of failure in obtaining the global minimum factor of safety.

3.3. The probabilistic optimisation methods

A new approach that employs probabilistic theory offers great promise in overcoming the problems of missing the global minima. The basic principle of probabilistic optimisation methods is to compare factors of safety of a large number of failure modes that are generated by random numbers. In essence it appears that the searcher is randomly walking in a domain that contains the critical failure mode. The ever-developing power of computers enables the searcher to evaluate the factor of safety for tens of thousands of failure modes in a few minutes. Consequently, in a probabilistic sense, the searcher has a good chance of approaching the global minimum purely due to the number of entries into the search area.

For the problem of concern, the upper and lower bound for each variable in Eq. (5), represented as χ_i^+ and χ_i^-, respectively, is set. A value of ith variable of χ for the jth random walk can be obtained and expressed by

$$\chi_i^j = \chi_i^- + r_i^j(\chi_i^+ - \chi_i^-), \tag{6}$$

where r_i^j is a random number ranged in (0,1).

Chen [15] found that this random trial method allows the searcher to evade local traps and hence to find the approximate location of the global minimum. This location is taken as the initial input of a subsequent deterministic search that accurately locates the minimum factor of safety. Greco [16] used a modified random approach that directed the search direction in a well-organised pattern. He claimed that an accurate solution could be obtained without the help of deterministic methods. Both works are concerned with the conventional 2D method of vertical slices. It has been found that difficulties in finding global minima are more challenging when the problem involves slices, or prisms, with non-vertical interfaces. More efficient and powerful optimisation methods are needed.

Recently a technique called the 'Simulated Annealing Method' has attracted significant attention [17,18]. This method has effectively solved the well-known 'travelling salesman' problem of finding the shortest cyclical itinerary for a travelling salesman who must visit each of N cities in turn. It is best explained through an analogy of cooling and annealing of metal. Physical annealing is a process in which a solid is heated until all particles randomly arrange themselves in the liquid state, followed by a slow cooling, spending a relatively long time to reach the freezing point. At higher temperature, the liquidised solid is allowed to move freely and reach thermal equilibrium. As the temperature is decreased slowly rather than quickly, nature is able to find the minimum energy level (freezing point). The traditional optimisation methods are similar to the quickly cooled process for a liquid metal, greedily searching for the minima in the downhill direction from the initial starting points. In a simulated annealing process, if ΔF, defined as $F(\chi_{j+1}) - F(\chi_j)$ in two consecutive random trials, is less than zero, χ_j will be replaced with χ_{j+1}. However, if $\Delta F > 0, \chi_{j+1}$ may still be accepted based on an auxiliary judgement. A random number r_i is generated in (0,1) and compared to the value $\exp[-\Delta F/T]$, where T is a specified parameter simulating temperature. If $r_i < \exp[-\Delta F/T]$, χ_j will be replaced with χ_{j+1}. The key issue is that the process is undertaken slowly with a large number of random trials so that the risk of mistakenly abolishing previous better

random trials has been reduced to a minimum. Even if this becomes a reality, there is a good chance that the better trial will be rescued by subsequent searches. The parameter T slowly controls this searching process and plays the role of the temperature similar to that in physical annealing.

The process starts from an initial temperature, T_0, which is set sufficiently high to allow uphill moves away from local minimal [17]. However, too high a temperature will result in deteriorating random steps that lower the efficiency. Recommendations for determining a reasonable starting temperature are therefore required. Before starting the simulated annealing, a number of random walks in accepted variable space (generally 100 or more) are generated to determine the maximum and minimum of the objective function, $F_{\max}$ and $F_{\min}$. The starting temperature T_0 is then defined by

$$T_0 = F_{\max} - F_{\min}. \tag{7}$$

The temperature during the optimisation is reduced by a damping function, that is,

$$T_k = T_0(\alpha_T)^k, \tag{8}$$

where T_k is the value of temperature at the kth step of cooling process. α_T is referred to as the temperature damping factor and falls in the range (0,1). α_T is chosen by trial and error [18]. m random steps are carried out in the kth step .

Bohachevsky et al. [19] proposed that the direction of a random step $\Delta\chi = \chi_{j+1} - \chi_j$ be determined by n random numbers $v = (v_1, v_2, \ldots, v_n)$ from the uniform distribution in $(-1, 1)$, which is converted into direction cosines $u = (u_1, u_2, \ldots, u_n)$,

$$u_i = \frac{v_i}{\left(\sum_{i=1}^{n} v_i^2\right)^{1/2}}. \tag{9}$$

To accommodate the irregularity of the optimisation variable domain, positive constants κ_i $(i = 1, \ldots, n)$ are proposed.

$$\kappa_i = \frac{(\chi_i^+ - \chi_i^-)}{\max\{(\chi_1^+ - \chi_1^-), \ldots, (\chi_i^+ - \chi_i^-), \ldots, (\chi_n^+ - \chi_n^-)\}} \quad (i = 1, 2, \ldots, n). \tag{10}$$

The magnitude of random step Δr decreases with temperature by a damping function, but remains constant at the temperature step T_k. The magnitude of random step Δr_k at T_k is defined as

$$\Delta r_k = \Delta r_0(\alpha_r)^{k-1}, \tag{11}$$

where α_r is the random step damping factor in the range (0,1). Δr_0 is the initial value of the random step, which is determined based on the properties of the objective function and the desired accuracy and resolution. Accordingly, the component of random step Δr_k in the direction of each variable is defined as

$$\Delta\chi_i = \kappa_i \Delta r_k u_i \quad i = 1, 2, \ldots, n \tag{12}$$

Example 1. An example explaining the simulated annealing process

Fig. 4(a) shows an example that has been documented in [4]. The homogeneous and weightless slope with $c = 750$ kPa, $\phi = 37^\circ$, $\chi = 35^\circ$, $\delta = 24^\circ$, is subjected to an inclined uniform load of 6228 kPa (as shown in Fig. 4(a)). Slip-line analysis results in a closed-form solution, $F_m = 1.0$ [20]. Although an accurate solution has been obtained previously [4], it was only obtained after a significant search effort with many unsuccessful trials. The simulated annealing method provides an alternative by which the local minima traps were avoided.

The slip surface is divided into five nodal points, A, B, C, D and E connected by smooth curves. Point A lies on the slope surface and provides one degree of freedom, the abscissa x_A; the x_i, y_i and δ_i associated with points B, C and D are varied during optimisation; Point E is fixed and no extra variable is provided. Therefore, in this case, there are in total 10 degrees of freedom: x_A, x_B, y_B, δ_B, x_C, y_C, δ_C, x_D, y_D, δ_D, which represent a kinematically admissible failure mode if constraint conditions are satisfied. Each segment of the slip surface is connected by two adjoining nodal points as shown in Fig. 4(a). In the simulated annealing method the following parameters were adopted: temperature damping factor $\alpha_T = 0.9$, random damping factor, $\alpha_r = 0.98$, and the number of random walks $m_k = 300$. Based on these selected parameters, 100 successful random steps yielded the starting temperature T_0. With the reductions of temperature and step magnitude through a large number of random steps the final solution was obtained. Fig. 4(b) and (c) show the variation of factor of safety in the process of optimisation based on the accepted random steps of $\Delta r_0 = 0.06$ and 0.27, which led to the minimum factors of safety of $F_m = 1.008$ and 1.001, respectively. It can be shown from Fig. 4(b) and (c) that unlike the conventional deterministic methods, the factors of safety sometimes increased during the process of minimisation but eventually approached the critical solution. The case $\Delta r_0 = 0.06$ was associated with $T_0 = 0.014$ and a larger factor of safety $F_m = 1.008$, compared to the case $\Delta r_0 = 0.27$ which was associated with $T_0 = 0.12$ and a more accurate result of $F_m = 1.001$.

4. Applications of the 3D slope stability analysis method

Example 2. Stability analysis of the Power Plant Slope of the Tianshengqiao II Project

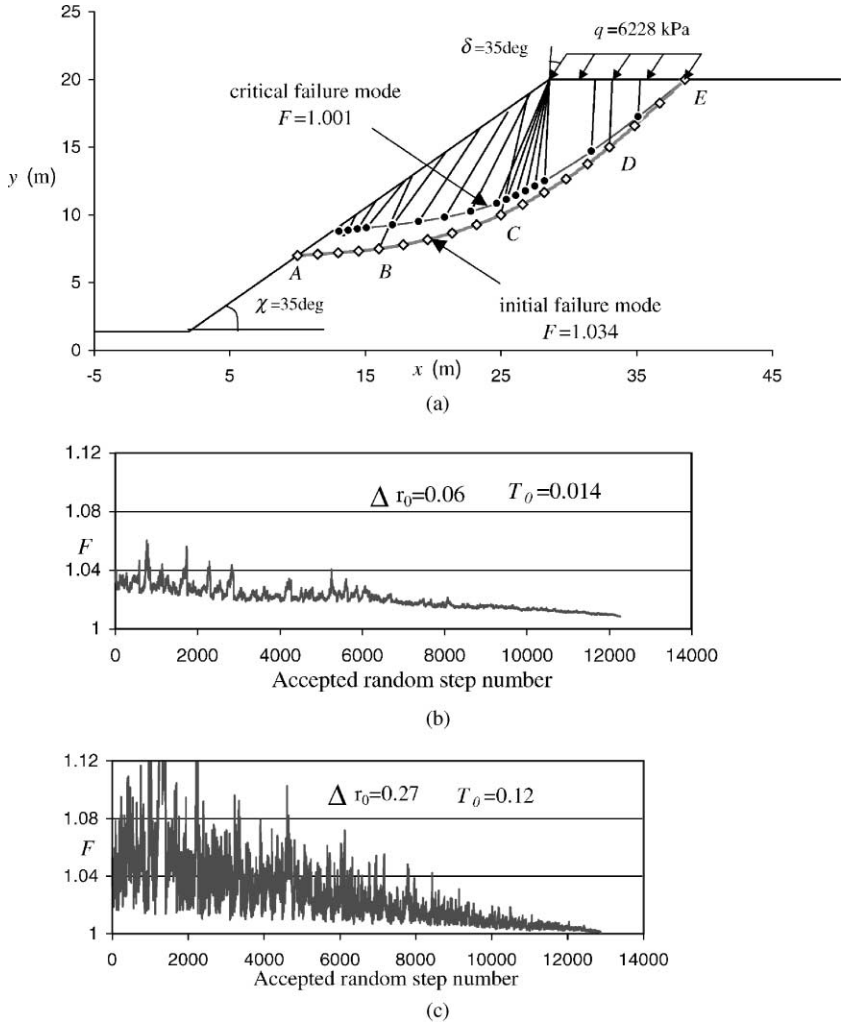

Fig. 4. Example 1: (a) the initial and critical failure modes of an example with closed-form solution; (b) variation of factor of safety with the process of optimisation for $\Delta r_0 = 0.06$; (c) variation of factor of safety with the process of optimisation for $\Delta r_0 = 0.27$.

This example illustrates the application of the computer program EMU-3D to a practical problem involving generalised topography, layered cross-sections and realistic ground water conditions.

The construction of the Tianshengqiao II Hydropower Plant resulted in an excavation of a 170 m high slope in a tertiary syncline formation consisting of interbedded sandstone and claystone. A large ground movement rate of 7.2 mm per day was observed in November 1986, following a 20 m deep excavation that daylighted a clay seam. The lateral borders of the unstable rock mass were clearly identified by two gullies that cut both sides of the slope. An extensive site investigation using boreholes allowed the failure plane to be identified as a clay seam that had formed on a bedding plane of the syncline formation. Fig. 5 shows the plan view of the geology. The boreholes also indicated a ground water level, some 5 m higher than the clay seam.

As this is a typical back analysis problem in which the slip surface is well defined, the failure mass was discretised using the type one process described earlier. The neutral plane was assumed to coincide with the axis of the syncline and three cross-sections adopted for the left side ($z < 0$) and five to the right ($z > 0$). Figs. 6 and 7 show the discretised failure mass in plan and the isometric view of the failure mass, respectively. Fig. 8 depicts the individual cross-sections. The geotechnical properties are described in Table 1. The factor of safety obtained by EMU-3D was 0.945.

For comparison, Table 2 shows the factors of safety of each cross-section assuming 2D conditions. The weighted average of the factors of safety is 0.885.

5. Extensions of the 3D slope stability analysis method

5.1. Stability analysis for arch dam abutments

The abutments of arch dams are subjected to large thrusts from the arch and generally require 3D analysis. The potential failure mass is in many ways similar to a

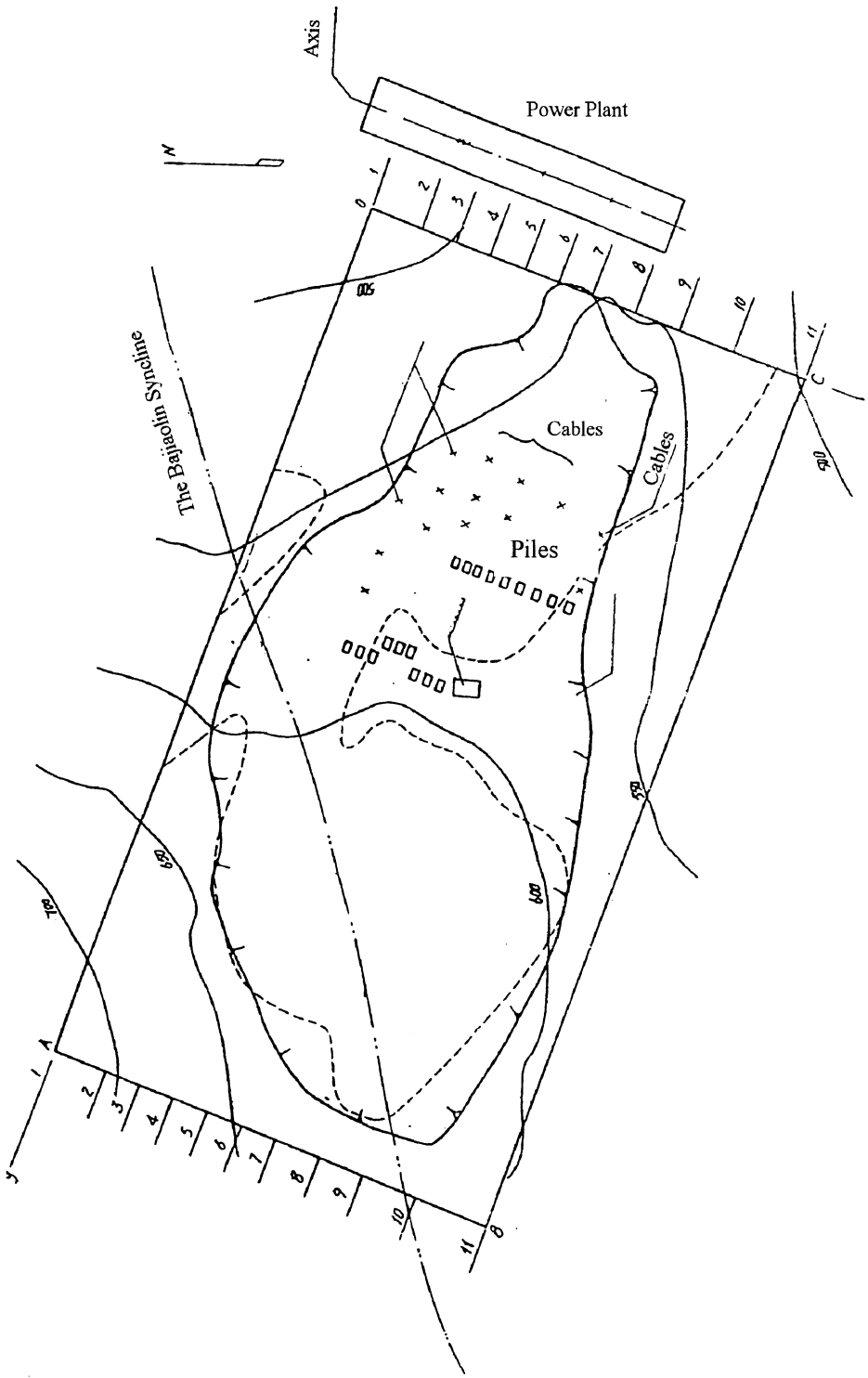

Fig. 5. The cross-sections that define the failure mass for example 2.

bearing capacity problem (Fig. 9(a)), except that it is rotated through 90° and only half of the problem needs to be considered. The surcharge acting on a footing in a bearing capacity problem is equivalent to the thrust acting on an abutment of a dam. The neutral plane for an arch dam is located at the lowest elevation of the abutment. The failure mass will diminish at a certain elevation of the abutment depending on the value specified for B in Eq. (1). In this particular case, a larger value of B does not necessarily result in a lower factor of safety since at higher elevations the thrust is lower and applied in a favourable direction as far as

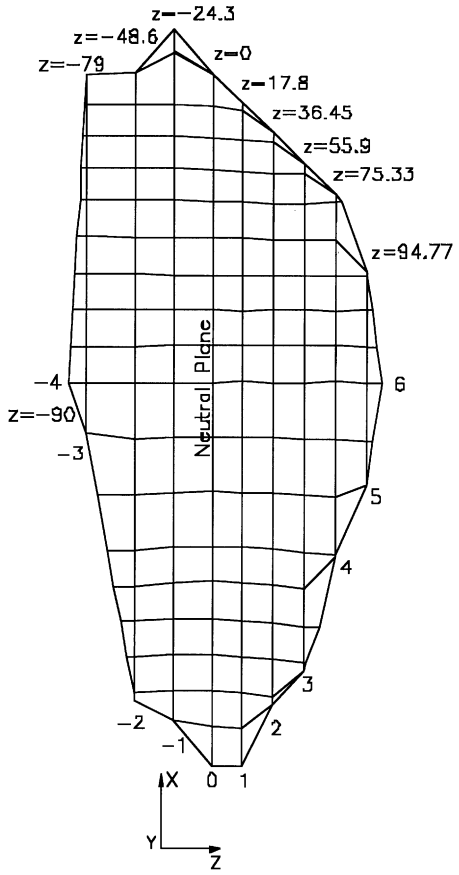

Fig. 6. A plan for the Tainshengqiao landslide discretisation.

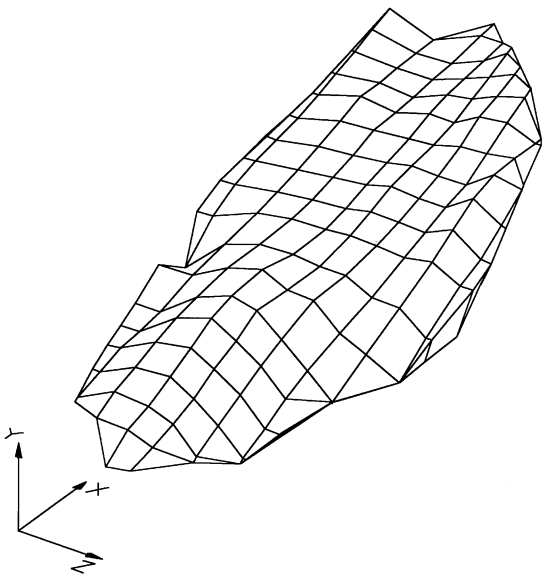

Fig. 7. The isometric view of the failure mass.

stability is concerned. A critical value of B may exist which gives the minimum value of F. This implies that only that part of the abutment lower than a specific elevation would slip under the application of the thrust.

Although there are many similarities to the bearing capacity problem, stability analyses of arch dam abutments involve a number of extra complexities that need special attention.

Firstly, the bench of the arch dam is not a rectangle and its location varies with elevation. A translation process is needed to ensure that the co-ordinates of the points produced by Eq. (1) are located correctly. Secondly, the directions of the row-to-row and column-to-column interfaces in the arch dam problem should coincide with the orientation (and spacing) of the geological discontinuities present within the rock mass. This can be achieved by introducing a process for rotating co-ordinates.

Example 3. Abutment stability of the Xiaowan Dam

Fig. 9 shows two typical horizontal cross-sections of the Xiaowan arch dam. The dam is 300 m high and transfers extremely high pressures to both abutments. The geology consists of granite with two joints striking virtually north–south and east–west and dipping almost vertically. It is quite convenient to align the co-ordinate system with the vertical and upward z-axis. The x-axis is aligned parallel to the river course but in the opposite direction to that of the stream flow. The horizontal cross-sections are '$z=$constant' interfaces and contain input information of the profile geometry and material properties. The joint sets that strike east–west serve as the row-to-row interfaces.

However, in addition to the two sets of vertically dipping joints, there exists in the rock mass another set of joints created as a result of relaxation during formation of the river valley. This set of joints, which is present on both left and right abutments, strikes approximately parallel to the river (i.e. along the x-axis) and dips into the river at an angle of 20–40°. The existence of this set of joints means that the abutment can slip along the relaxation joints towards the river. The 3D stability analysis should be based on a velocity field that can accommodate movement in the negative x direction, produced by the arch thrust and in the positive y direction along the relaxation joints, caused by gravity. The $y-z$ plane is therefore rotated to create a new co-ordinate system $x-y'-z'$ such that all the "$z'=$constant" planes are parallel to the relaxation planes as shown in Fig. 10. The input geometry and the applied arch thrusts also need to be resolved into the new co-ordinate system. Fig. 11 shows the "$z'=$constant" cross-sections based on the original "$z=$constant" cross-sections. Fig. 12 shows a front view of the thrust force.

Isometric views of the initial and critical failure modes are shown in Fig. 13(a) and (b), respectively. The corresponding factors of safety are 4.02 and 3.61, respectively. The value of B is 89 m, which means that

the failure mass includes the part of the abutment between the upper point of exit of the failure surface at 1170 m elevation and the bottom at 1245 m elevation. The geotechnical parameters are listed in Table 3. It should be emphasised that this analysis has been conducted on the basis of traditional concrete dam design. Such designs usually specify an allowable factor of safety of 3.5 for arch dam abutments, with assumed values of cohesion and friction angle based on contributions from both intact rock bridges and joints.

Table 4 lists the factors of safety for $B = 44$, 63, 89 and 108 m. These correspond to upper failure surface exit points with elevations of 1090, 1130, 1170, and 1210 m, respectively. As expected, it was found that there exists a value of B which results in a minimum factor of safety; i.e. $B = 89$ m corresponding to a failure surface exit elevation of 1170 m.

5.2. Slope stability analysis at a tunnel portal

It is widely understood that selecting a stable portal is of vital importance in tunnel excavation. The stability of a portal exhibits typical 3D features. Firstly, cutting a vertical front face may cause instability despite only a limited width of the slope toe being excavated. Using the conventional 2D slope stability analysis that assumes an infinite length of the front face may be too conservative. Secondly, failure may take place as the portal is further weakened during tunnel excavation that results in the rock mass hanging on the ceiling of the tunnel. Obviously, it is impossible to model this failure process by 2D analysis. The following example explains how modelling this process can be made possible by the 3D approach described in this paper.

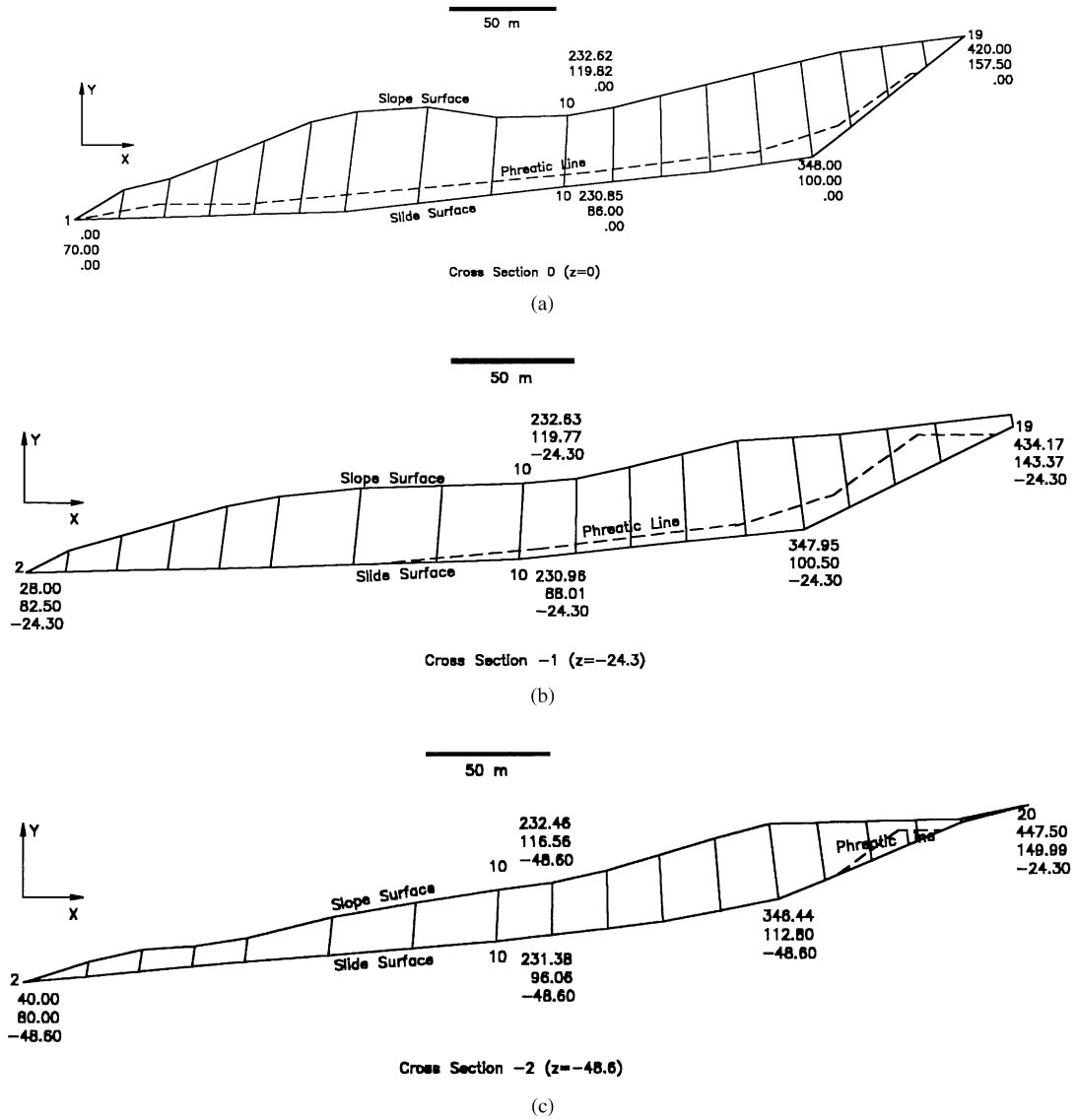

Fig. 8. (a–i) Cross-sections of the Tainshengqiao landslide.

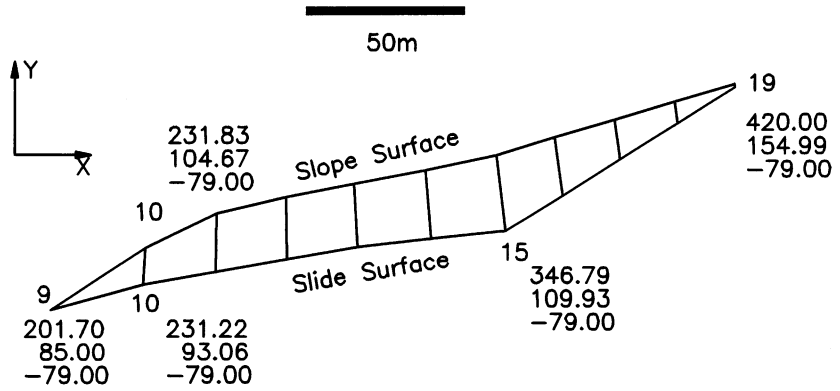

Cross Section −3 (z=−79)

(d)

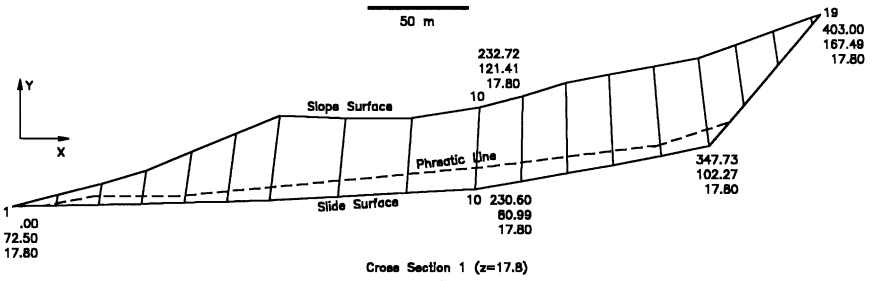

(e)

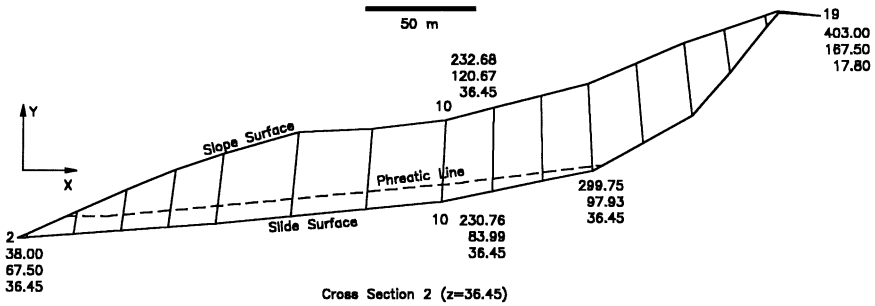

(f)

Fig. 8. Continued.

Example 4. Portal stability analysis of the Hongjiadu Hydropower Project, China

This project involves a 182 m high rockfill dam, with all of the water discharge facilities located in the left limestone abutment. Unfortunately, the dip direction of the bedding planes coincides with that of the abutment slope (Fig. 14). Stability of the slope during excavation of the portals of various water release tunnels has been of serious concern.

Fig. 14 shows a geological cross-section of the flood discharge tunnel. Investigation has identified several weak seams that have developed along the bedding planes. These seams will daylight when the front face is excavated. The factor of safety along seam AA′ that daylights at elevation 1106.0 m will be considerably reduced if 2D analysis is employed since the shear strength parameters of AA′ are very low. As a result, it may be necessary to specify that significant reinforcement be utilised in order to excavate the portal safely.

However, the front face is only 9.4 m wide. The slip surface, in addition to AA′, must involve the side faces that intercept the rock mass which has significantly higher shear strength parameters. Therefore, the 3D factor of safety of this failure mode may be somewhat higher than that predicted from 2D analyses, thereby reducing the requirement for reinforcement.

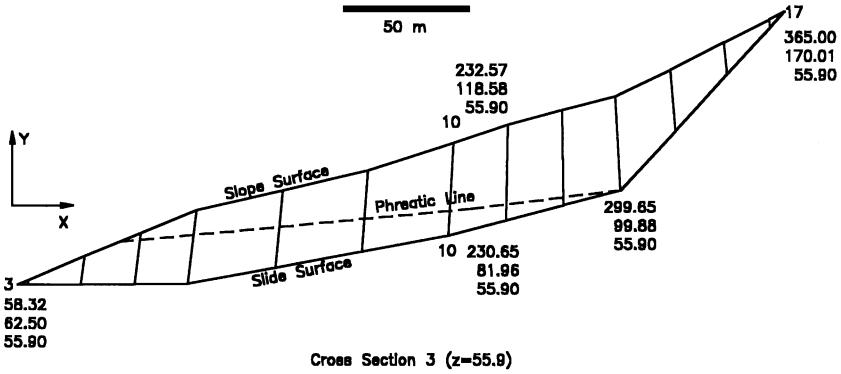

(g)

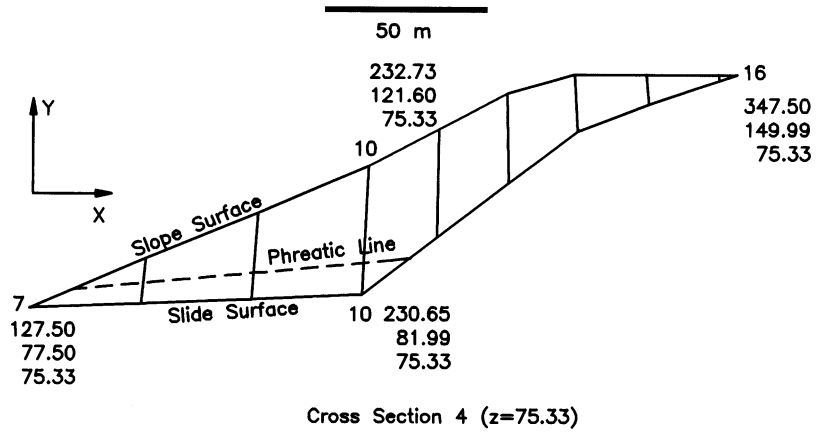

(h)

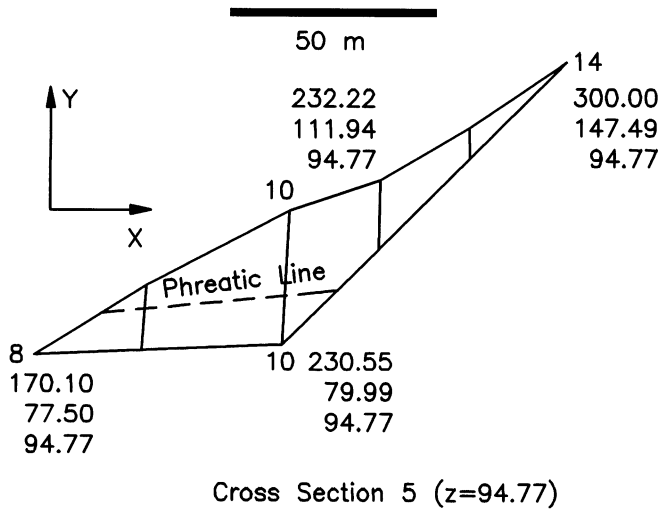

(i)

Fig. 8. Continued.

Fig. 15 shows the critical slip surface obtained by a global failure mode that takes AA′ as its basal failure surface with its side faces intercepting the rock mass. In the calculation, the shear strength parameters of the weak plane AA′ are $\phi = 21.8^\circ$ and $c = 50\,\text{kPa}$ while those for the rock mass are $\phi = 30.0^\circ$ and $c = 500\,\text{kPa}$ (refer to Table 5). These values were derived using the empirical criterion of Hoek and Brown [22]. The rock mass has two sets of steeply dipping joints that are adopted as the row-to-row and column-to-column interfaces, in which the row-to-row interfaces have slightly in-dipping angles of 10°. In this case, the

Table 1
Geotechnical parameters of the rock mass material for the Tianshengqiao Project

	Front part			Rear part		
	c (MPa)	tan ϕ	γ (g/cm^3)	c (MPa)	tan ϕ	γ (g/cm^3)
Weak seam	0.01	0.14	2.25	0.015	0.17	2.25
Rock mass	0.2	0.26	2.3	0.02	0.26	2.3

Table 2
The factors of safety for individual cross-sections and their weighted average

Number	−3	−2	−1	0	1	2
F	0.630	0.909	1.204	0.997	0.883	0.795
Number	2	3	4	5	Weighted average	
F	0.795	0.573	0.464	0.524	0.885	

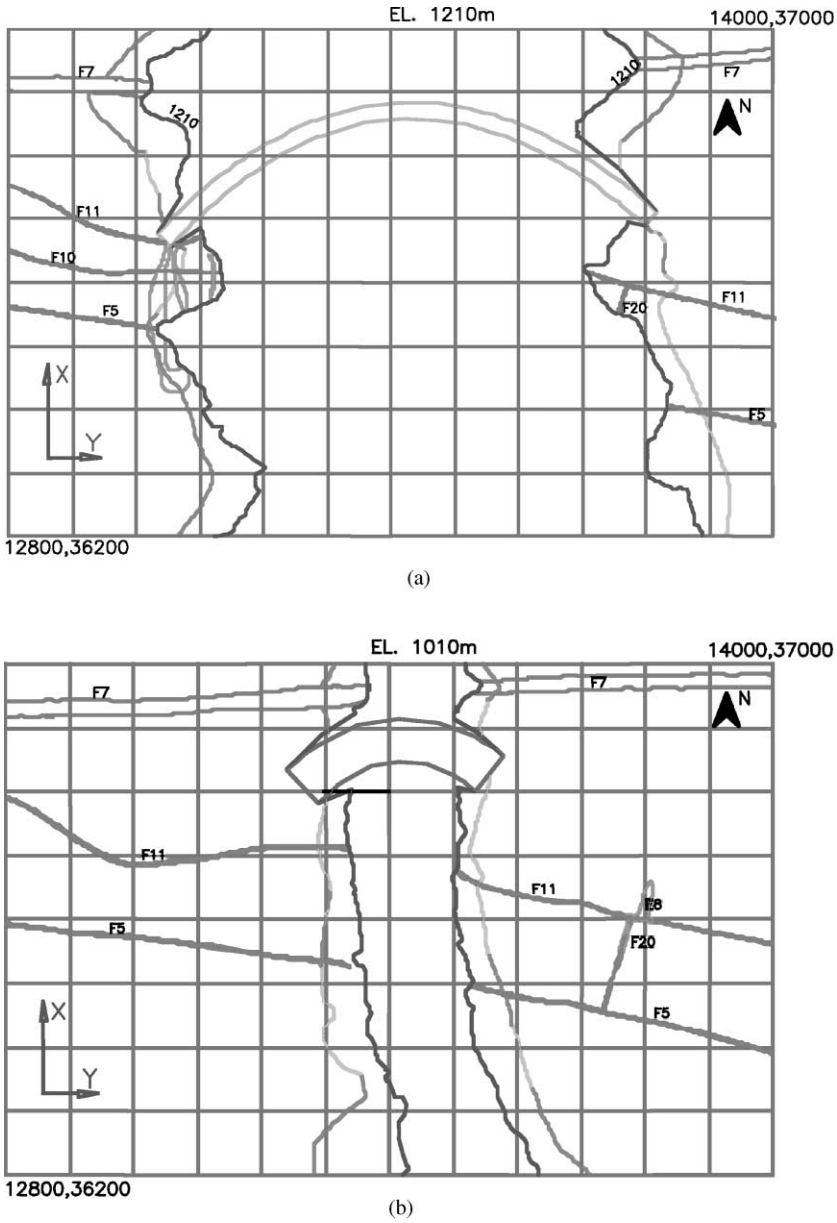

Fig. 9. Typical horizontal cross-sections of the Xiaowan arch dam at: (a) elevation 1210 m and (b) elevation 1010 m.

bedding plane AA′ that forms the basal plane of the failure surface is constructed by connecting four nodal points as shown in Fig. 16. Since AA′ is well defined, x_i and y_i in Eq. (4) are all fixed. The values of δ_i are also fixed, being -10° to model the in-dipping joints. ω is taken as unity, representing a set of vertically dipping joints. Only ζ of the four nodal points will be varied during the optimisation process. The failure mode represented by Eq. (1) was slightly modified to produce a planar basal failure surface. The critical slip surface

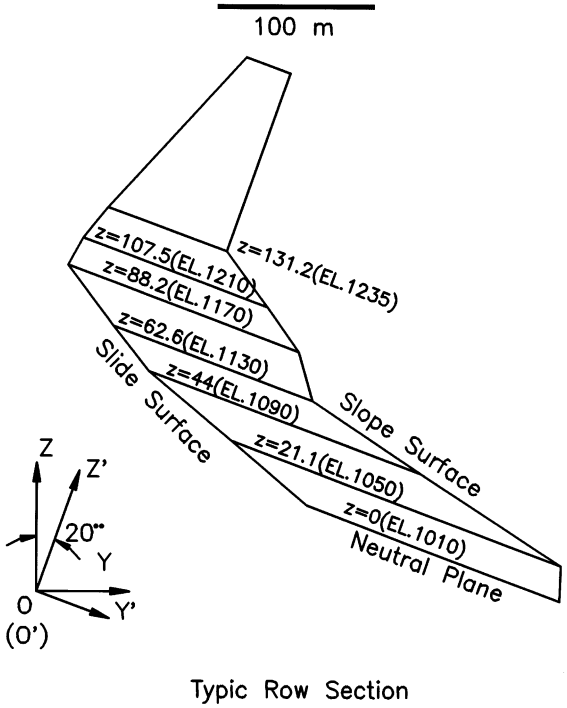

Fig. 10. Rotation of the $y-z$ plane to bring the '$z=$constant' planes parallel to the relaxation joints.

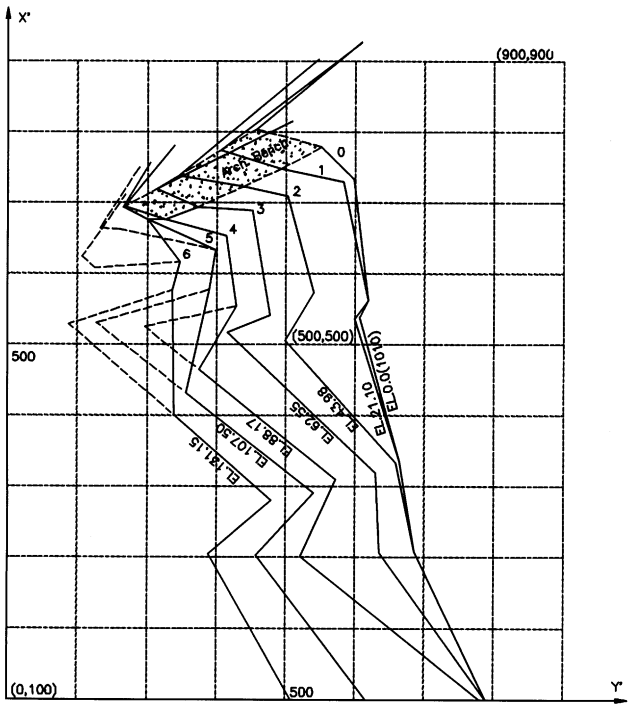

Fig. 11. The '$z'=$constant' cross-sections after rotation of the original 'z=constant' cross-sections.

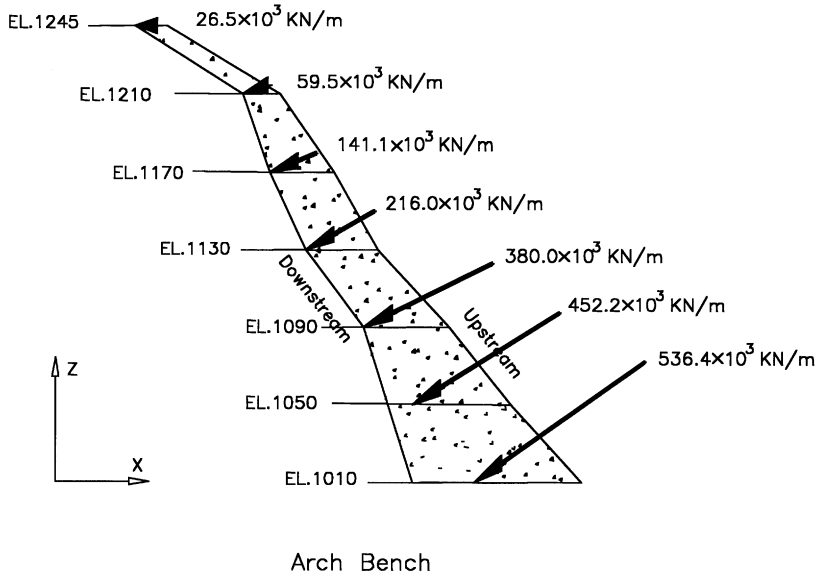

Fig. 12. A front view of the thrust force.

shown in Fig. 15 is plotted based on the right partial prisms. The view shown is that from upstream to downstream. The minimum factor of safety associated with this critical slip surface is 2.890, which is reasonably high. In this case if a 2D approach is employed, the factor of safety is only 1.096, as shown in Fig. 16.

In view of the large factor of safety associated with the 3D planar failure surface mode, it was suspected that the conventional slope stability analysis using a curved slip surface might still control the stability of the slope [21]. Figs. 17 and 18 compare the critical curved slip surfaces obtained from 2D and 3D approaches. The slip surface at the neutral plane, as well as that in 2D analysis, was created by connecting three nodal points, shown as A, B, C in Fig. 17, using a spline function. It can been seen that by considering the 3D effects, the

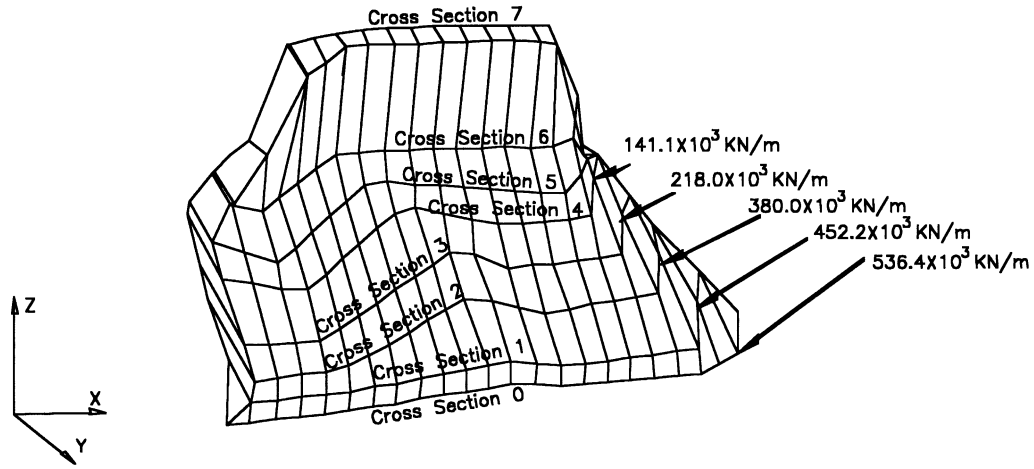

(a)

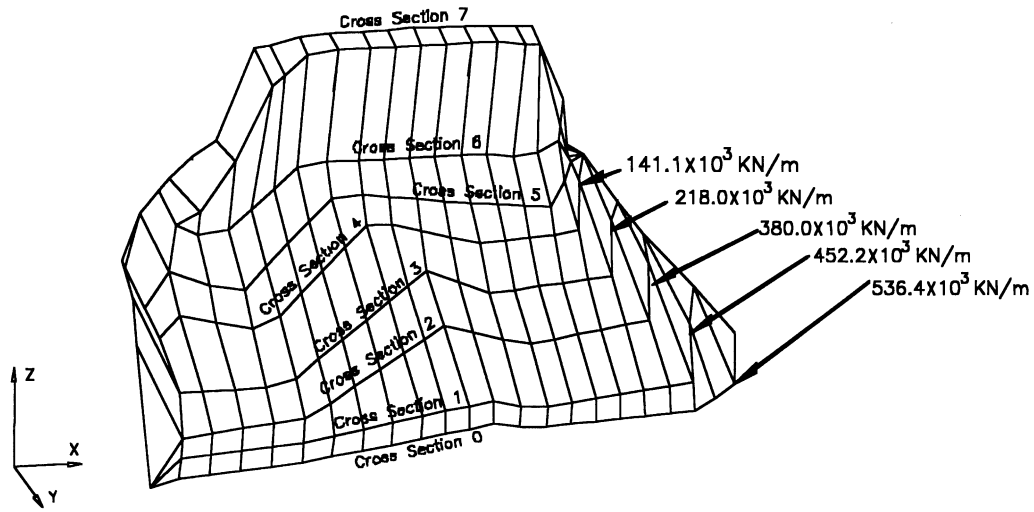

(b)

Fig. 13. Isometric views of the initial and critical failure modes. (a) the initial, $F_0 = 4.02$; (b) the final, $F_m = 3.61$.

Table 3
Geotechnical properties of the rock mass of the Xiaowan arch dam abutment

Shear surfaces	Geological features	ϕ (°)	c (MPa)
Slip surface	A combination of rock bridges and joints striking north–south	20	1.5
Row-to-row interfaces	A combination of rock bridges and joints striking east–west	20	1.5
Column-to-column interfaces	Relaxation joints	30	0.1

factor of safety is raised by 50% from $F_2 = 1.777$ to $F_3 = 2.419$. In the case of 3D analysis, the value of $B/2$ in Eq. (1) has been taken as 4.7 m to model the width of the portal opening. The variables included in the optimisation process were x_B, y_B, x_C, y_C, and ζ_B, ζ_C. The location of A is fixed at the toe and ζ_A is kept at unity to accommodate a fixed width of the portal opening. Therefore, x_A, y_A, and ζ_A remain unchanged during the optimisation process. Points B and C can move freely in the x and y directions, thus each involves two degrees of freedom. However, they are constrained to move in 90° and 30°, respectively to the horizontal in the calculation. This would minimise the total number of degree of freedom without too much loss of accuracy [13]. Table 6 shows the initial input and optimised output of these variables and the associated factors of safety.

Table 4
The factors of safety for $B = 44$, 63, 89 and 108 m

B (m)	44	63	89	108
Elevation of the point of the upper exit (m)	1090	1130	1170	1210
Factor of safety	3.72	3.63	3.61	3.70

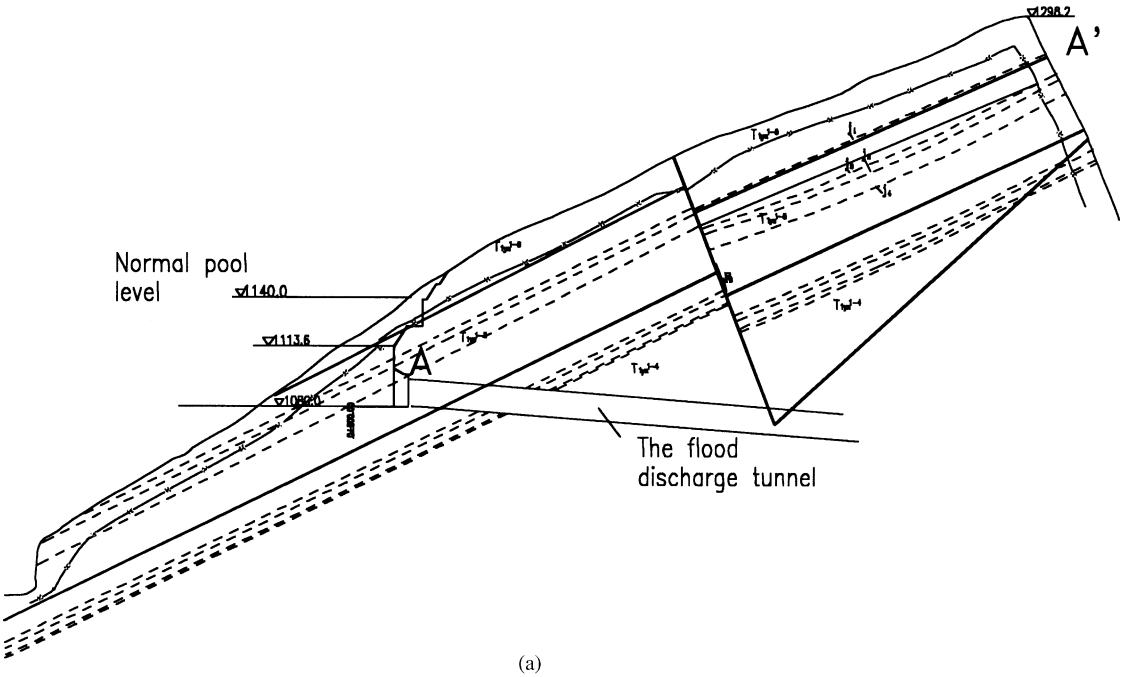

(a)

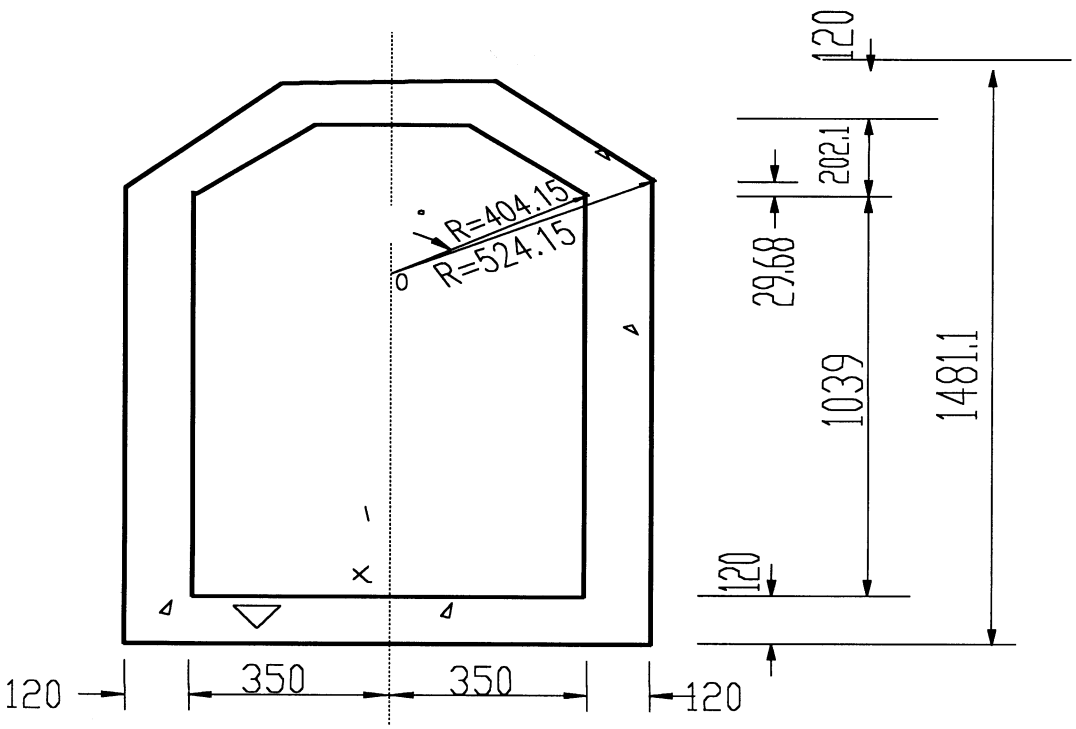

(b)

Fig. 14. The Hongjiadu Project: (a) geological cross-section of the flood discharge tunnel; (b) the cross-section of the tunnel.

It can also be seen that the minimum factor of safety for the curved slip surface ($F = 2.419$) is lower than that of the planar basal slip surface ($F = 2.890$) obtained using the parameters listed in Table 5.

The next step of calculation proceeds with the excavation of the tunnel, which causes some of the prisms to hang over the ceiling of the opening. This unique procedure can only be made possible in a 3D analysis. However, some assumptions regarding the velocities of the hanging prisms are necessary. In the approach adopted here it is assumed that all the hanging prisms move as a rigid body, with a direction parallel to the neutral plane and inclined at an angle ψ to the base of the first non-hanging prism on the neutral plane (refer to

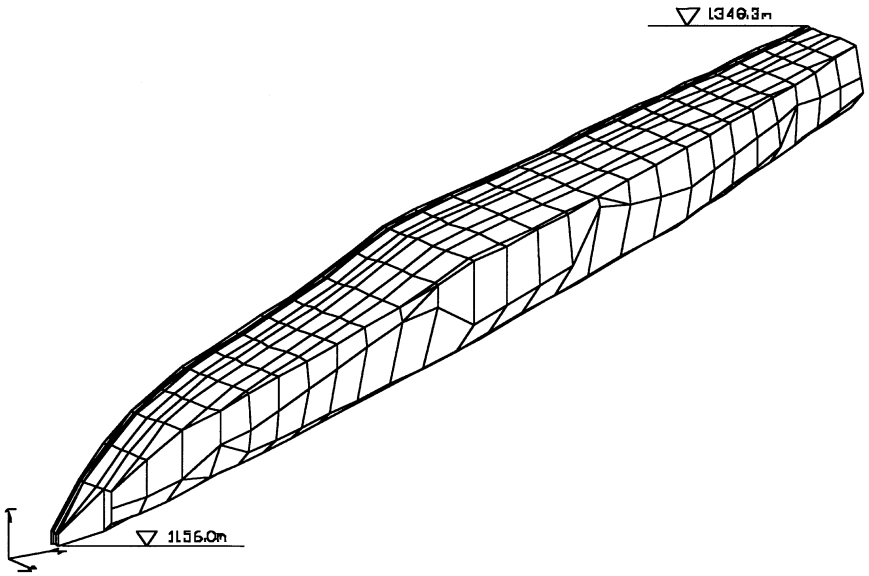

Fig. 15. The critical slip surface obtained from the three-dimensional stability analysis for planar slip surface along the weak seam AA′, $F = 2.890$.

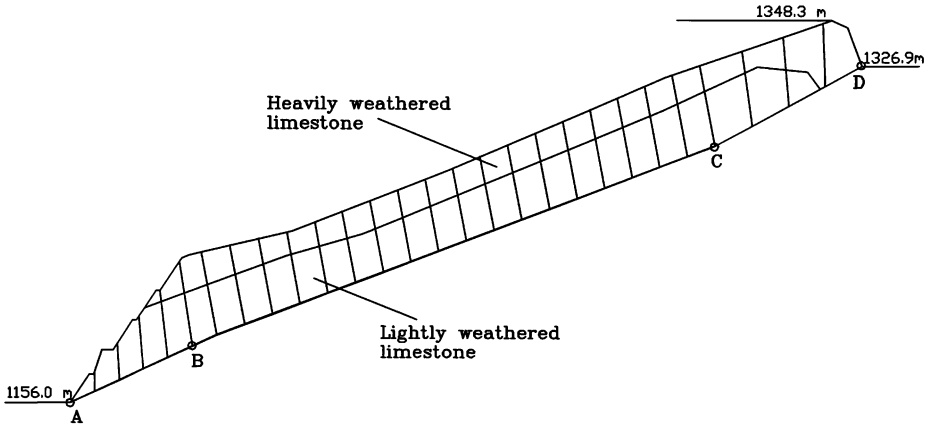

Fig. 16. The two-dimensional stability analysis for the planar slip surface along week seam AA′, $F = 1.096$.

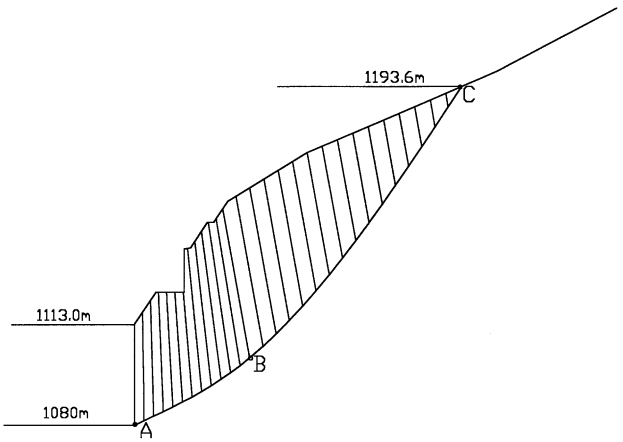

Fig. 17. The two-dimensional stability analysis for curve slip surface, $F = 1.777$.

Fig. 19). ψ is determined so that it offers the lowest factor of safety. However, the actual implementation involves a reduction of $\tan\psi$ by F in order to give consistent weighting among various slip surfaces during the optimisation process. That is, for the slope under consideration, a value of ψ' for any slip surface is assumed, but the input of ψ for a particular slip surface is related to its factor of safety based on the following equation:

$$\tan\psi = \frac{\tan\psi'}{F}. \tag{13}$$

The calculation starts from an initial estimate and concludes at an optimised solution as shown in Table 7. Fig. 20 shows the critical slip surface with an associated minimum factor of safety of $F = 2.058$. The calculation is based on comparing different

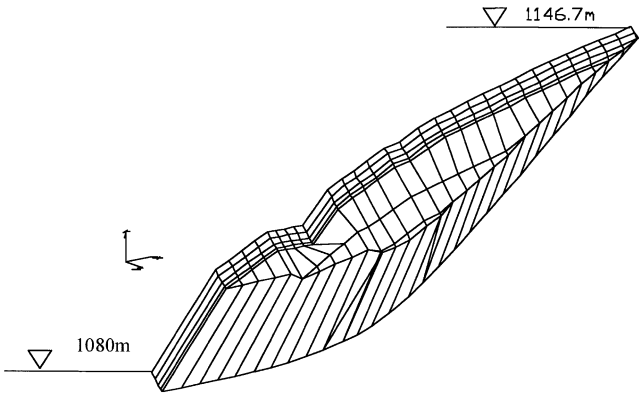

Fig. 18. The critical slip surface obtained from the three-dimensional stability analysis for curve slip surface, an oblique view, $F = 2.419$.

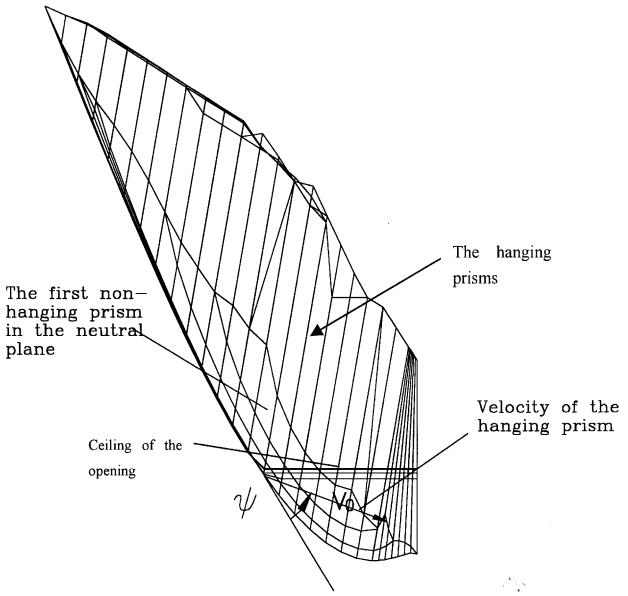

Fig. 19. Cross-section at the neural plane, looking from the left.

assumed values of ψ, which confirmed that taking a ψ' close to zero always gave smaller factors of safety. By comparing Fig. 21 to Fig. 18, it can be observed that the critical failure surfaces before and after tunnel excavation have similar elevations at the crown, indicating that a similar volume of the failure mass is involved. However, the case with the tunnel opening has a 'flatter' shape near the toe, which appears reasonable, considering the existence of the free face provided by the tunnel side walls, that allow more rock to fall from both sides.

Obviously, the procedures described herein do not replace the conventional procedures of assessing the stability of underground openings, but instead provides a method for evaluating the influence of the tunnel on the stability of a slope weakened by the excavation of the tunnel.

6. Future developments

In spite of the successes so far achieved, the method is still in the early stages of development. Much more work is required before the full potential of the method can be realised.

- More numerical work is needed to upgrade the discretisation process. As can be seen in the figures presented in this paper, the edge prisms created by the present program result in a relatively ragged boundary to the failure mass. Algorithms that are capable of offering automatic discretisation with little distortion, for all kinds of practical problems, are required.
- The implementation of the method is occasionally hampered by convergence problems while solving for the velocities of particular prisms from

Table 5
Geotechnical properties of rock material in the portal stability analysis

Shear surfaces	Geological features	ϕ (°)	c (MPa)
Slip surface	A combination of rock bridges and joints	30	0.5
Weak seam AA′	Clay seam along the bedding plane	21.8	0.05
Row-to-row interfaces	A set of in-dipping joints	20	0.2
Column-to-column interfaces	Another set of vertically dipping joints	20	0.2

Table 6
The initial input and optimised output of the curve slip surfaces[a]

Nodal point	A			B			C			F
	x_A	y_A	ζ_A	x_B	y_B	ζ_B	x_C	y_C	ζ_C	
Initial	0.00	0.00	1.000	28.4	40.00	1.039	56.77	91.70	0.739	3.608
Final	0.00	0.00	1.000	28.4	25.24	1.154	69.74	99.19	0.651	2.419

[a] Note: x_A, y_A are in metres.

Table 7
The initial input and optimised output of the slip surfaces after tunnel excavation

Nodal point	A			B			C			F
	x_A	y_A	ζ_A	x_B	y_B	ζ_B	x_C	y_C	ζ_C	
Initial	0.00	0.00	1.000	8.08	2.41	1.036	33.29	54.48	0.628	2.559
Final	0.00	0.00	1.000	8.08	−1.42	1.319	45.68	61.63	0.620	2.058

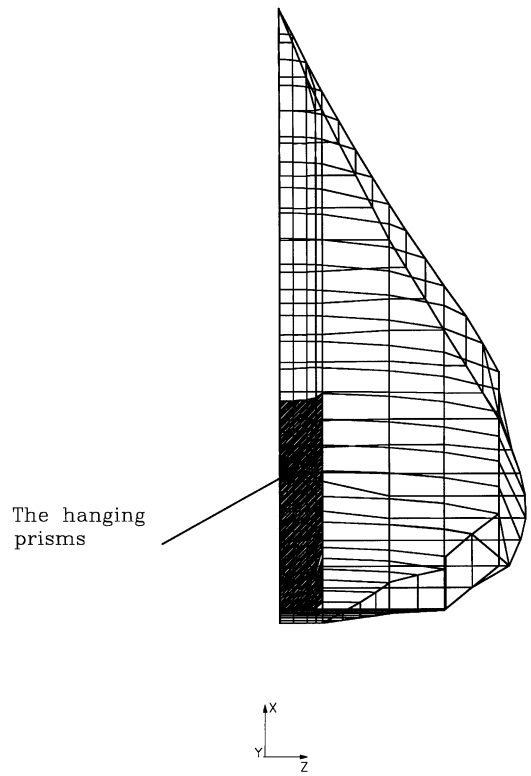

Fig. 20. An overview of the critical slip surface with tunnel opening.

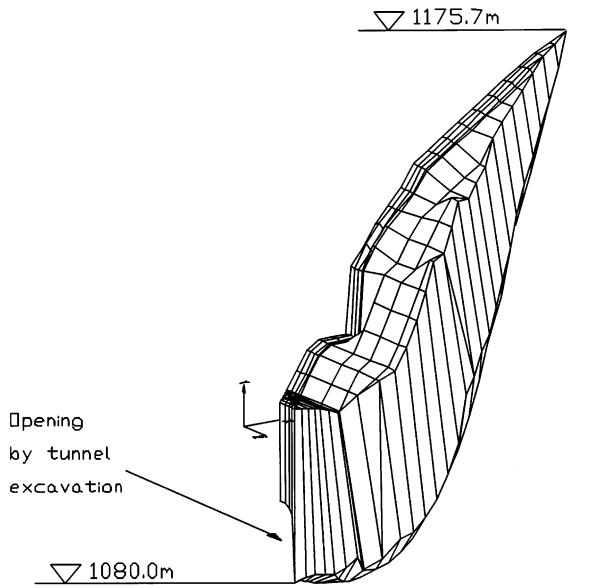

Fig. 21. The critical slip surface with tunnel opening, a front view, $F = 2.058$. (Note: only the right half prisms of the failure mass are shown in the figure.)

Eqs. (20)–(22)—see Part I of the paper. This problem is usually connected with: (1) large friction angles; (2) incompatible directions between normals to the slip surface and interfaces of adjacent prisms; and (3) insufficient numerical power in solving the non-linear equations. These problems are currently under consideration and should be solved in the near future.

- As the method offers an upper bound solution, the development of powerful optimisation routines is of utmost importance.
- In addition to the two types of discretisation patterns proposed in this paper, further approaches are needed to extend the applicability of this method to, for example, the analysis of rock block systems.

7. Conclusions

The principles and analytical approaches described in PART I of this paper require numerical support that consists of: (1) a generalised pattern to model three-dimensional slip surfaces, (2) powerful optimisation routines to find critical failure modes, and (3) easy input and output facilities capable of interpreting and displaying the complicated topography and geology and slip surface.

The examples presented in this paper show that these problems can be reasonably solved. However, more work is required to modify EMU-3D so that a three-dimensional slope stability analysis program with high efficiency and extensive applicability can be eventually made possible.

Inputting the 3D topography and stratified profile by cross-sections provides a simple method of dealing with practical three-dimensional problems. Only a small amount of additional work over two-dimensional analysis is required for the analyses.

As numbering of prisms is automatically carried out by the computer program, the preparation of a data file is only a matter of several hours of work. Typically, once the input data has been input, each analysis only consumes a few minutes of computer time.

The discretisation patterns described in the paper offers sufficient flexibility to model a wide range of failure modes, such as the potential failure mass of a tunnel portal or the abutment of an arch dam. Applications to both problems have been described in this paper. It also permits the search for critical failure surface to be implemented in the rational framework provided by optimisation theory.

The use of the method and the associated program has been demonstrated through a number of practical examples, which clearly demonstrate the potential of this method in solving problems that otherwise would not be possible if two-dimensional approaches are employed.

Acknowledgements

The financial support of this project provided by the following Institutions is gratefully acknowledged: (1) China National Natural Science Foundation, grant No. 59493600, (2) Hong Kong Polytechnic University, the RGC grant (PolyU 5065/97E) of the University Grants Committee of the Hong Kong SAR Government of China, and (3) the Small Grant Scheme of the Australian Research Council.

References

[1] Zhang X. Three-dimensional stability analysis of concave slopes in plan view. ASCE J Geotech Eng 1988;114:658–71.
[2] Leshchinsky D, Baker R, Silver ML. Three-dimensional analysis of slope stability. Int J Numer Anal Meth Geomech 1985;9: 199–223.
[3] Lam L, Fredlund DG. A general limit equilibrium model for three-dimensional slope stability analysis. Canad Geotech J 1993;3:905–19.
[4] Donald I, Chen ZY. Slope stability analysis by the upper bound approach: fundamentals and methods. Canad Geotech J 1997;34:853–62.
[5] Nelder JA, Mead R. A simplex method for function minimization. Comput J 1965;7:308–13.
[6] Hooke R, Jeeves TA. 'Direct search' of solution of numerical and statistical problems. J Assoc Comput Mech 1961;8:212–29.
[7] Powell MJD. An efficient method for finding the minimum of a function of several variables without calculating derivatives. Comput J 1964;7:155–62.
[8] Davidon WC. Variable metric method for minimization. Argonne National Laboratory, AEC R&D Report ANL-5990 (Rev.), 1959.
[9] Fletcher R, Powell MJD. A rapid convergent method for minimization. Comput J 1963;6:163–8.
[10] Baker R, Garber M. Variational approach to slope stability. Proceedings of the Nineth International Conference on Soil Mechanics and Foundation Engineering, Tokyo, Vol. 2/3, 1977. p. 9–12.
[11] Baker R. Determination of critical slip surface in slope stability computations. Int J Numer Anal Meth Geomech 1980;4:333–59.
[12] Celestino TB, Duncan JM. Simplified search for noncircular slip surface. Proceedings of the 10th International Conference on Soil Mechanics and Foundation Engineering, Stockholm, Vol. 3, 1981. p. 391–4.
[13] Li KS, White W. Rapid evaluation of the critical slip surface in slope stability problems. Int J Numer Anal Meth Geomech 1987;11:449–73.
[14] Chen ZY, Shao CM. Evaluation of minimum factor of safety in slope stability analysis. Canad Geotech J 1988;25:735–48.
[15] Chen ZY. Random trials used in determining global minimum factors of safety of slopes. Canad Geotech J 1992;29:225–33.
[16] Greco VR. Efficient Monte Carlo technique for locating critical slip surface. J Geotech Eng ASCE 1996;122(GT7):517–25.
[17] Kirkpatrick S, Gelatt Jr. CD, Vecchi MP. Optimization by simulated annealing. Science 1983;220(4598):671–680.
[18] Bohachevsky IO, Johnson ME, Stein ML. Generalized simulated annealing for function optimization. Technometrics 1986;28(3): 209–17.
[19] Vanderbilt D, Louie SG. A Monte Carlo simulated annealing approach to optimization over continuous variables. J Comput Phys 1984;56:259–71.
[20] Sokolovski VV. Statics of soil media. Butterworth, London, 1960 (Translated by Jones DH, Scholfield AN).
[21] Hoek E, Bray JW. Rock slope engineering. The Institute of Mining and Metallurgy, 1977.
[22] Hoek E. Estimating Mohr-Coulomb friction and cohesion values from the Hoek–Brown failure criterion. Int J Rock Mech Min Sci 1990;27:227–9.